Thin Solid Films 602 (2016) 84–89

Contents lists available at ScienceDirect

Thin Solid Films

journal homepage: www.elsevier.com/locate/tsf

Evidence of strong spin–orbit interaction in strained epitaxial germanium

C. Morrison, J. Foronda, P. Wiśniewski, S.D. Rhead, D.R. Leadley, M. Myronov

Department of Physics, University of Warwick, Coventry CV4 7AL, United Kingdom

ARTICLE INFO

Article history:
Received 22 May 2015
Received in revised form 28 September 2015
Accepted 28 September 2015
Available online 3 October 2015

Keywords:
2D hole gas
Germanium
Quantum wells
Mobility
Reduced pressure-chemical vapour deposition
Rashba spin–orbit interaction

ABSTRACT

Spin–orbit interaction effects are of great interest, primarily for the ability to modulate spin transport in a semiconductor channel for device applications. In particular, the Rashba spin–orbit (S–O) interaction allows for a tuneable spin modulation response dependent on the applied electric field, which can be achieved using standard semiconductor gate technology. We present evidence of the Rashba S–O interaction in two modulation doped germanium (Ge) quantum well (QW) heterostructures with different layer structures, and consequently different band structures and internal electric fields across the QW region. We show that two complementary low temperature magnetotransport analyses can be used to identify and quantify the Rashba S–O parameter in these materials, although quantification is limited in one case due to significant parallel conduction. We highlight that both techniques (Weak Antilocalisation and Shubnikov de-Haas oscillations) should be used when analysing a new material system as other conduction and magnetoresistive effects can obscure evidence of the Rashba S–O interaction in one or both of these regimes.

1. Introduction

Germanium quantum well (QW) heterostructures have been studied over the past 20 years, primarily for the interesting physical effects that can be observed in the 2D hole gas formed in the QW [1–6]. Recently, extremely high hole mobilities have been achieved in this material system both at low temperatures (1.3×10^6 cm^2/Vs) [7] and room temperature (4500 cm^2/Vs) [8,9]. Because of these advances Ge QW heterostructures now look like strong candidates for high mobility electronic applications such as field effect transistors (FETs), especially due to the highest mobility structures being grown by an industrial type equipment (reduced pressure chemical vapour deposition (RP-CVD)) onto standard Si (001) substrates. Since the proposal of the spin FET in 1990 by Datta and Das [10], semiconductor materials have been studied for their spin–orbit interactions, particularly those that can be modified by an applied electric field, such as the Rashba spin–orbit (S–O) interaction [11], in order to create devices that utilise spin modulation and control to perform logic operations. Recently, evidence has begun to emerge of a strong Rashba S–O interaction in Ge QWs [12–14]. In particular, Ge QWs offer an excellent opportunity to study the cubic Rashba interaction in a material in which the Dresselhaus spin–orbit interaction due to bulk inversion asymmetry [15] is absent.

We examine the use of two complementary magnetotransport analyses for identifying and quantifying the Rashba S–O interaction in Ge. We find that both techniques are essential and either or both can be used to study the Rashba S–O interaction, dependent on other material parameters which may obscure the characteristic magnetotransport features associated with the Rashba S–O interaction. We present a detailed effective mass and scattering parameter analysis for two Ge QW heterostructures. Finally, we examine the material parameters that affect magnetotransport in Ge QWs and propose reasons the Rashba S–O effect is or is not observed, and the ideal system for studying these effects.

2. Experimental details

The Ge heterostructures studied here were grown by reduced pressure chemical vapour deposition (RP-CVD) onto standard 100 mm diameter (001) Si substrates. The layer structures of the two heterostructures (hereby referred to as sample 1 and sample 2, exhibiting parallel conduction at all temperatures) are shown schematically in Fig. 1(a) and (b), respectively. First, a 600 nm Ge layer was grown, followed by a reverse linearly graded (RLG) buffer of SiGe down to 80% Ge ($Si_{0.2}Ge_{0.8}$) over a thickness of 1600 nm [16]. At this point the growth of the two samples differs. For sample 1, a 10 nm Boron (B) doped $Si_{0.2}Ge_{0.8}$ region was grown next, followed by a $Si_{0.2}Ge_{0.8}$ spacer of 20 nm. Onto this spacer an 11 nm pure Ge quantum well (QW) was grown, which was then capped with 30 nm $Si_{0.2}Ge_{0.8}$ and 2 nm of Si. This structure is known as an inverse modulation doped heterostructure due to the remote doping layer being located below the QW channel. For sample 2, a 22 nm pure Ge QW was grown directly onto the RLG buffer, followed by a spacer of 20 nm

E-mail address: M.Myronov@warwick.ac.uk (M. Myronov).

http://dx.doi.org/10.1016/j.tsf.2015.09.063
0040-6090/

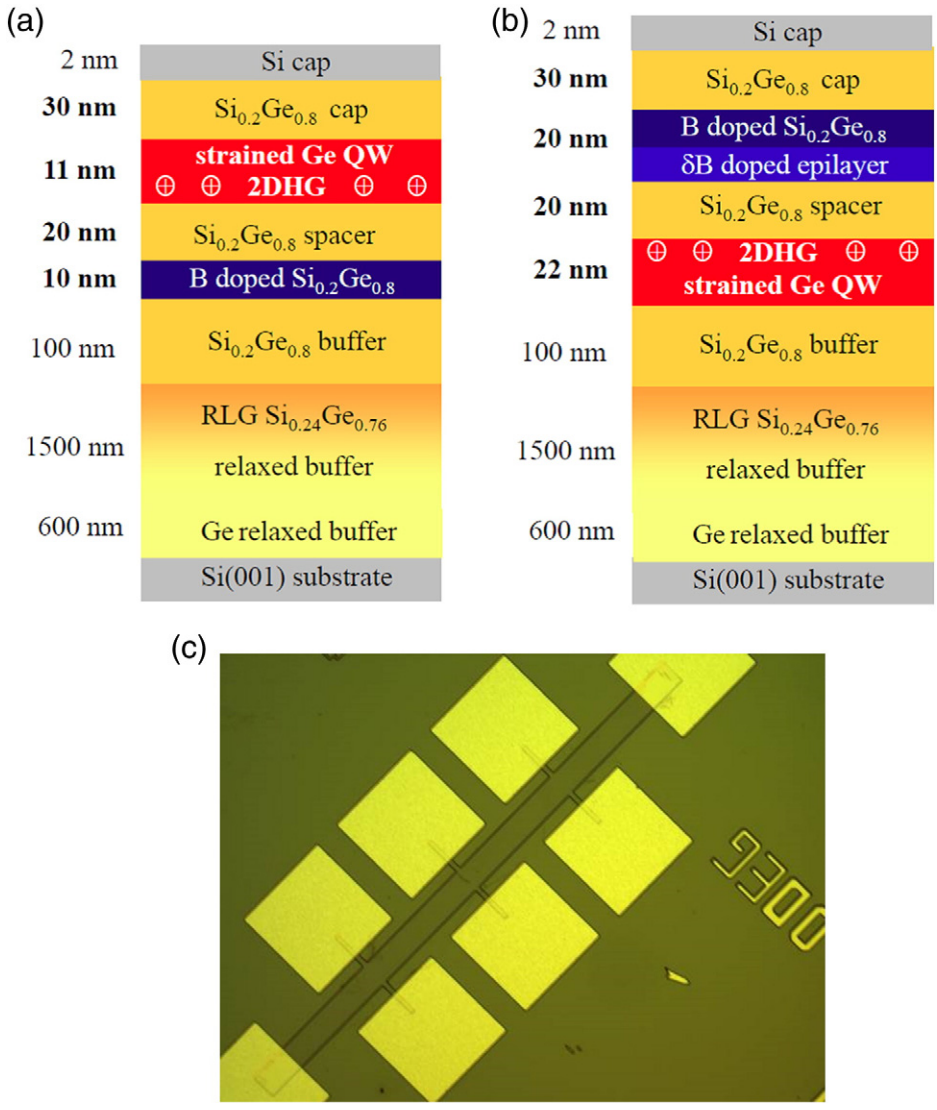

Fig. 1. (a) Layer structure of sample 1. (b) Layer structure of sample 2. (c) Optical image of an example Hall bar device fabricated on sample 2.

$Si_{0.2}Ge_{0.8}$. A delta layer of B was then grown, followed by a further 20 nm $Si_{0.2}Ge_{0.8}$ doped with B. Sample 2 was then capped with 30 nm of undoped $Si_{0.2}Ge_{0.8}$ and 2 nm of Si.

Hall bar devices were fabricated on both samples using the same process. First, contact pads were defined using photolithography and metallised with Al or Au/Ag deposited by thermal evaporation. The mesa region was then defined with photolithography and a dry plasma etch in SF_6 with a small percentage of O_2 was used to etch the heterostructure down to the Si substrate. An image of one of the fabricated Hall bar devices is shown in Fig. 1(c). Finally, the devices were annealed at 425 °C for 25 min for Al contacts or 300 °C for 30 min for Au/Ag contacts to diffuse the metal down through and below the Ge QW to form an ohmic contact directly to the layer. While this results in contact to all of the upper layers in the heterostructure, these layers freeze out at low temperatures leaving transport only in the QW. This is evidenced by metallic transport behaviour where a constant, high mobility is measured at temperatures below 20 K (450,000 cm^2/Vs for sample 1 and 777,000 cm^2/Vs for sample 2) with a constant carrier density (5.9×10^{11} cm^{-2} for sample 1 and 1.9×10^{11} cm^{-2} for sample 2). If Ohmic contact is not made to the QW region then we instead observe freeze out at low temperatures and a large increase in sheet resistance corresponding to transport through a semiconducting region at low temperature.

Low temperature magnetotransport measurements were performed in an Oxford Instruments Heliox AC-V ^{3}He cryostat with a base temperature of 0.3 K and maximum magnetic field of 12 T and a Quantum Design Physical Property Measurement System with ^{3}He insert with a base temperature of 0.4 K and maximum magnetic field of 9 T. Longitudinal (R_{xx}) and transverse (R_{xy}) resistances were measured using either a Stanford Research Systems SR830 lock-in amplifier or a LakeShore Model 372AC resistance bridge. In both cases an applied current of 100 nA was used at a frequency of 19.77 Hz.

3. Magnetotransport properties

Low temperature magnetotransport measurements are shown in Fig. 2 for sample 1 (2(a)) and sample 2 (2(b)). Clear Shubnikov de-Haas (SdH) oscillations are visible for both heterostructures, arising from Landau level quantisation under the applied magnetic field. For sample 1, the SdH oscillations display a structure that deviates from that expected from integer Landau level formation at finite temperature (i.e. a damped sinusoid), displaying instead a 'beating' structure with

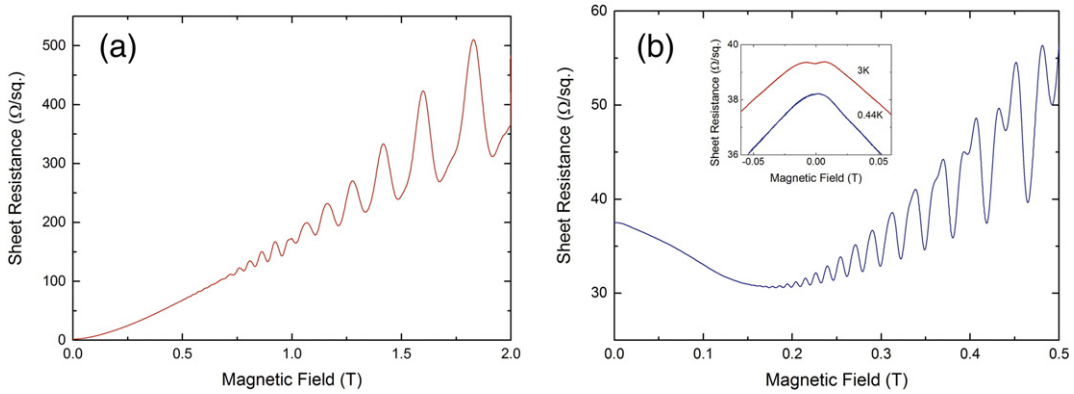

Fig. 2. Magnetoresistance as a function of applied magnetic field for (a) sample 1 and (b) sample 2 at a temperature of 0.4 K. Shubnikov de-Haas oscillations are observed in both materials, but beating is only observed for sample 1. Sample 2 displays a clear signature of localisation effects near zero field (inset to (b)).

clear nodes at 0.65 T and 1.00 T. This structure is initial evidence of each Landau level being split into two, fully spin polarised energy levels separated by the Rashba spin–orbit (S–O) energy. This may be confirmed by performing a Fast Fourier Transform (FFT) of magnetoresistance as a function of inverse magnetic field to determine the frequency spectrum of the oscillations. Each frequency corresponds to a distinct energy (or carrier density) of holes within the QW. For the relatively small perturbation induced by the Rashba S–O interaction we should observe two closely separated peaks in the spectrum. An FFT of the lowest temperature curve is shown in Fig. 3. Two clear peaks are observed at frequencies of 11.4 T and 13 T. These peaks can be attributed to spin down and spin up carriers, respectively, and the frequency values may be converted to carrier density using the relation $p = \frac{fe}{\pi\hbar}$. This yields spin down and spin up carrier densities $p_{\downarrow} = 5.53 \times 10^{11}\ \mathrm{cm}^{-2}$ and $p_{\uparrow} = 6.31 \times 10^{11}\ \mathrm{cm}^{-2}$, respectively. These values are located symmetrically around the Hall carrier density for the QW taken from the Hall resistivity (R_{xy}), $5.9 \times 10^{11}\ \mathrm{cm}^{-2}$ as expected for Rashba S–O perturbation of the QW sub-band.

To aid further analysis of these effects, it is important to determine the effective carrier (hole) mass m^* for carriers in each QW. This may be achieved by measuring the amplitude of the SdH oscillations as a function of magnetic field and temperature, effectively determining the degree of damping which is dependent on the effective mass.

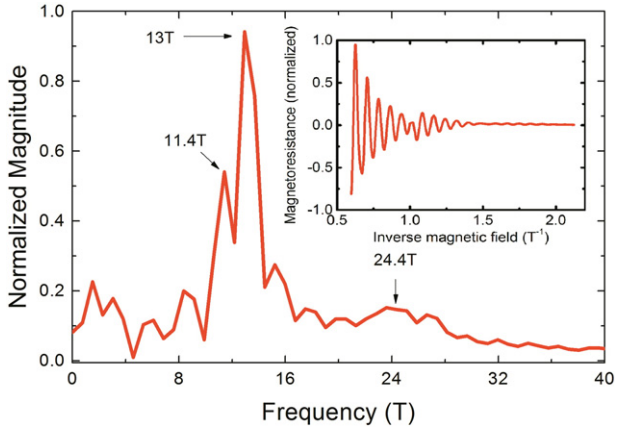

Fig. 3. Fast Fourier Transform of the low field magnetoresistance of sample 1 (up to 1.7 T) as a function of inverse magnetic field (see inset). The first two peaks close to 12 T correspond to the oscillations due to the spin split hole population — the second at 24 T is the peak due to the sum of the spin sub-bands. Inset: Magnetoresistance at 0.4 K plotted as a function of inverse magnetic field for the region 0–2 T.

Shubnikov de-Haas oscillations of Rashba spin–split holes may be described by the following equation,

$$\frac{\Delta\rho_{xx}(B)}{\rho_{xx}(0)} = 4\cos\left(\frac{2\pi m^*\left(E_F \pm \beta_{SO}{k_F}^3\right)}{\hbar eB}\right)\exp\left(-\frac{\pi m^*\alpha_D}{eB\tau_t}\right)\frac{\psi}{sinh(\psi)} \quad (1)$$

where E_F is the Fermi energy, α_D is the Dingle ratio $(\frac{\tau_t}{\tau_q})$, where τ_t is the transport scattering time and τ_q is the quantum scattering time, β_{SO} is the cubic Rashba spin–orbit parameter and

$$\psi = \frac{2\pi^2 k_B T m^*}{\hbar eB} \quad (2)$$

In the low field regime this may be approximated to [17]

$$\frac{\Delta\rho_{xx}(B)}{\rho_{xx}(0)} = 4\cos\left(\frac{2\pi m^* E_F}{\hbar eB}\right)\exp\left(-\frac{\pi m^*\alpha}{eB\tau_t}\right)\frac{\psi}{sinh(\psi)} \quad (3)$$

Eq.(3) may be solved iteratively to determine the two unknown parameters, the effective mass and the Dingle ratio [18]. The two curves involved in this iterative process are plotted in Fig. 4, applied to the data from sample 1, for an effective mass $m^* = 0.095 \pm 0.010\ m_0$ and a Dingle ratio $\alpha_D = 48 \pm 3$. Determining the effective mass in this sample is non-trivial through standard analysis of the peak amplitude as a function of temperature, due to the non-monotonic behaviour of the amplitude as a function of field. The physical interpretation of the peaks at a higher magnetic field, after closure of the first beat, is complicated by the presence of the Rashba spin splitting. In order to determine the effective mass, the lowest field peaks have to be used, before the interference of the two frequencies generates the first beat. This is the region in which Eq. (3) is obeyed and is indicated in Fig. 4(a) and (b) by dashed red lines. Because of this limitation on the analysis the value we determine will be less accurate than for magnetotransport data with a single oscillation frequency. Analysis of this region yields the above mentioned effective mass and Dingle ratio.

Determining the effective mass for sample 2 is more straightforward, as no beating effect is observed and the oscillations evolve monotonically in the applied magnetic field. The curves used for the analysis are shown in Fig. 5, for the final convergence of the iterative process at an effective mass $m^* = 0.065 \pm 0.005 m_0$ and a Dingle ratio $\alpha_D = 18 \pm 2$. These parameters, including the extracted quantum and transport lifetimes, are summarised in Table 1.

With the effective mass determined, the Rashba S–O parameter and the associated energy can now be calculated. The Rashba interaction is cubic in k-space for heavy holes, which are the only carrier types here

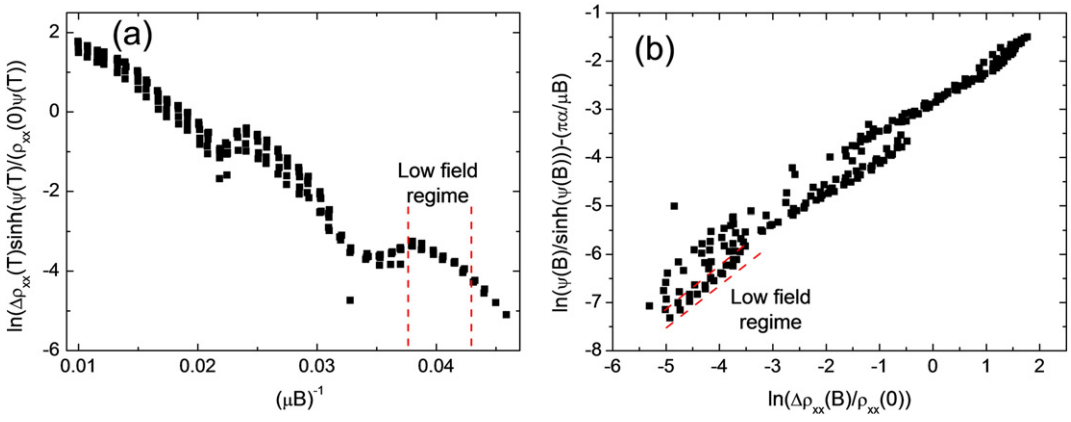

Fig. 4. (a) and (b) Plots of transformed data using Eq. (1) for effective mass analysis of sample 1. These plots show the final iteration giving the solution of $m^* = 0.095$ and $\alpha = 47.6$. Because of the beating effect observed, only the lowest field peaks are used for the analysis, as highlighted in the figure.

due to the effect of strain on the band structure, and so the following equation may be used [19]

$$\beta_{SO} = \sqrt{\frac{2}{\pi}}\frac{\hbar^2}{2m^*}\frac{p(p_+ - p_-) + \Delta p(p_+ + p_-)}{6p^2 + 2\Delta p^2} \tag{4}$$

where $p_\pm = \sqrt{p \pm \Delta p}$, Δp is the difference between the spin up and spin down sub-band hole densities and p is the sum of the spin up and down hole densities. Inserting the values for the spin sub-band densities for sample 1 and the effective mass gives a Rashba spin–orbit parameter $\beta_{SO} = 1.0 \pm 0.6 \times 10^{-28}$ eVm^3, and a corresponding spin splitting energy $2\beta_{SO}k_F^3$ of 1.4 ± 0.9 meV at the Fermi wave vector $k_F = 1.93 \times 10^8$ m^{-1}.

Sample 2 does not exhibit beating of the SdH oscillations. However, a temperature dependent magnetoresistance contribution is observed, centred on zero field (inset, Fig. 2(b)). At the lowest temperatures, up to 1 K, negative magnetoresistance is observed. This is typically associated with Weak Localisation (WL) of carriers arising from the interference of coherent partial electron waves upon scattering events forming closed loops. At temperatures above 1.9 K, a positive magnetoresistance region is observed, associated with Weak Anti-Localisation (WAL), a correction to the WL effect arising from the Rashba S–O interaction. Therefore, the Rashba S–O interaction is still observable in sample 2, albeit via a different method of analysis. The quantum correction to the magnetoresistance exhibits an anomalous temperature dependence that is attributed to WL contributions from the parallel conducting layers in sample 2 and the Ge QW, and WAL arising from the QW only. Fig. 2(b) appears to have WL at low temperatures transitioning to WAL at higher temperatures, opposite to what is expected in terms of WL/WAL behaviour. This is in reality the result of a combination of resistivity from the high mobility Ge quantum well and a lower mobility parallel conducting δ-doped SiGe layer. It can be assumed that the transport parameters for the two layers are significantly different as we expect high mobility transport in the high quality QW (observed in similar samples) and a low mobility in the SiGe:B layer where there is considerable impurity scattering. The variation of parameters (τ_t, τ_φ (phase breaking scattering time), τ_{SO} (spin–orbit scattering time)) which govern WL/WAL will produce effects with different magnitude and temperature dependences. This difference can produce what may look like a transition from WL to WAL with increasing temperature when not considering the presence of parallel conduction.

It is interesting to examine the reasons for our inability to observe beating in the SdH oscillations for sample 2. The amplitude of the oscillations at any given field and temperature is a function of two key material parameters, the quantum lifetime and the effective mass of holes in the quantum well. One hypothesis would be that the SdH oscillations in sample 2 are damped to the extent that any beats are unobservable, or require a high enough magnetic field that they are obscured by the onset of Zeeman splitting. However, both damping terms in Eq. (1) indicate that the damping of oscillations should be lower for a sample with lower effective mass and higher quantum lifetime, such as sample 2 (relative to sample 1). We must therefore look elsewhere for an explanation. The onset of Zeeman splitting in sample 2 is very quick, occurring at fields of only 0.3 T, compared to 1.7 T in

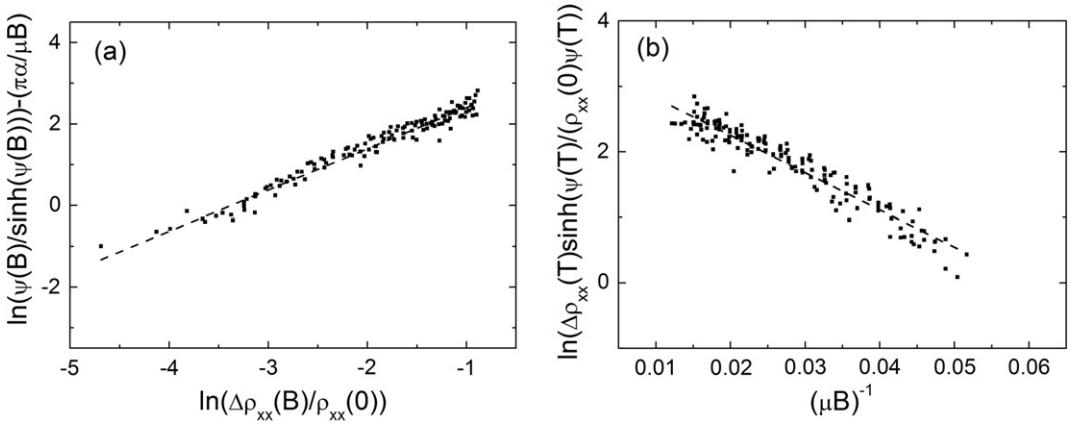

Fig. 5. (a) and (b) Plots of transformed data using Eq. (1) for effective mass analysis of sample 2. These plots show the final iteration giving the solution of $m^* = 0.065$ and $\alpha = 18.1$.

Table 1
Summary of the material parameters as measured for samples 1 and 2.

Sample	Hall mobility (0.3 K) (cm^2/Vs)	Hall carrier density (cm^{-2})	Effective mass (m_0)	Transport lifetime (0.3 K) (ps)	Quantum lifetime (ps)
1	450,000	5.9×10^{11}	0.095	24	0.5
2	780,000	2×10^{11}	0.065	29	1.6

sample 1. It is therefore likely that any beating in sample 2 occurs long after the peaks begin to split due to the Zeeman energy, resulting in a complex oscillation spectrum which cannot be analysed for the Rashba S–O parameter. We can examine this hypothesis by plotting the sum of two instances of Eq. (1) with energy separated by the Rashba S–O energy, using the measured material parameters for sample 2, to simulate the position of the first observable node in the SdH oscillations. This is shown in Fig. 6, assuming a similar Rashba S–O energy to sample 1 as the two heterostructures should exhibit a similar electric field across the QW. From this simulation we can see that the first beat is only 5% of the sheet resistance, which may not be observable in the AC magnetotransport measurement. Ideally we need materials with a low Landé g-factor to minimise the Zeeman splitting energy, making the first Zeeman split peaks occur beyond the first beats. For some samples it may be possible to resolve the spin split peaks even in the presence of Zeeman splitting (as in, for example, p-type GaAs/InGaAs quantum wells [20]). However, for the case of the Ge quantum wells studied here, this was not possible, and when the Zeeman-split oscillations were analysed no statistically significant spin–split peaks was observed and only a single peak was observed at the Hall carrier density. A detailed study of the Landé g-factor as a function of heterostructure design and band structure therefore appears to be essential. Recent developments in THz cyclotron resonance offer a way of measuring the Rashba S–O parameter without the problems associated with Zeeman splitting [21]. Another alternative is to use WAL, but a more complex theoretical treatment is required for systems such as that reported here.

4. Summary

In summary, we have shown that the Rashba S–O interaction in strained Ge quantum well heterostructures can be identified and quantified using two complementary low temperature magnetotransport techniques — Weak Antilocalisation and Shubnikov de-Haas (SdH) oscillation frequency analysis. In the case of sample 1, clear beating in the SdH oscillations is observed corresponding to pairs of split Landau levels separated by a Rashba S–O energy of 1.4 meV. Sample 2 exhibits significant parallel conduction, due to the existence of a highly B-doped channel which does not freeze out even at low temperatures.

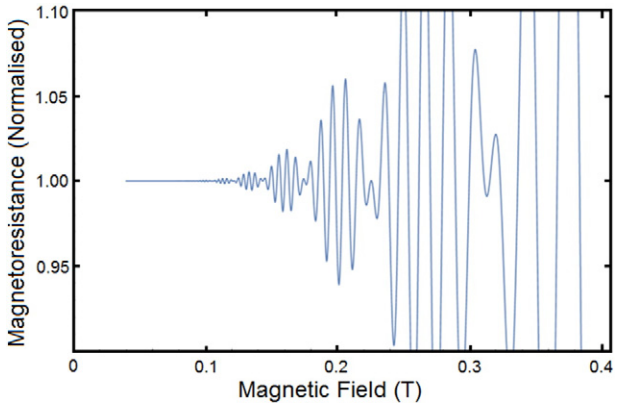

Fig. 6. Simulation of Shubnikov-de Haas oscillations using Eq. (1) for the material parameters from sample 2. The first beats before the onset of Zeeman splitting (not shown) at 0.3 T are only a few percent of the sheet resistance.

No evidence is found via SdH oscillations of the Rashba S–O interaction, at least before the onset of significant Zeeman splitting which may obscure the effect. However, a clear effect is observed at lower magnetic fields, with local minima in magnetoresistance at zero field corresponding to weak anti-localisation. These observations highlight the need to examine both regions in the magnetoresistance carefully, as evidence of the Rashba S–O interaction may be obscured in one regime by other magnetoresistance effects or distortions due to parallel conduction in the structure. The change in the observed effects between the two samples clearly shows the large changes achievable in magnetoresistance phenomena even between two nominally similar structures, which may be attributed to the changes in the band structure of the QW region and the effective electric field across the QW.

Acknowledgements

This work was supported by the EPSRC funded “Spintronic device physics in Si/Ge Heterostructures” EP/J003263/1 and “Platform Grant” EP/J001074/1 projects.

References

[1] C.M. Engelhardt, D. Többen, M. Aschauer, F. Schäffler, G. Abstreiter, E. Gornik, High mobility 2-D hole gases in strained Ge channels on Si substrates studied by magnetotransport and cyclotron resonance, Solid State Electron. 37 (1994) 949–952.
[2] M. Myronov, T. Irisawa, O.A. Mironov, S. Koh, Y. Shiraki, T.E. Whall, E.H.C. Parker, Extremely high room-temperature two-dimensional hole gas mobility in Ge/$Si_{0.33}Ge_{0.67}$/Si(001) p-type modulation-doped heterostructures, Appl. Phys. Lett. 80 (2002) 3117.
[3] B. Rößner, G. Isella, H.V. Känel, Effective mass in remotely doped Ge quantum wells, Appl. Phys. Lett. 82 (2003) 754.
[4] B. Rössner, D. Chrastina, G. Isella, H. von Känel, Scattering mechanisms in high-mobility strained Ge channels, Appl. Phys. Lett. 84 (2004) 3058.
[5] K. Sawano, Y. Kunishi, Y. Shiraki, K. Toyama, T. Okamoto, N. Usami, K. Nakagawa, Magnetotransport properties of Ge channels with extremely high compressive strain, Appl. Phys. Lett. 89 (2006) 162103.
[6] M. Myronov, D.R. Leadley, Y. Shiraki, High mobility holes in a strained Ge quantum well grown on a thin and relaxed $Si_{0.4}Ge_{0.6}$/LT-$Si_{0.4}Ge_{0.6}$/Si(001) virtual substrate, Appl. Phys. Lett. 94 (2009) 092108.
[7] A. Dobbie, M. Myronov, R.J.H. Morris, A.H.A. Hassan, M.J. Prest, V.A. Shah, E.H.C. Parker, T.E. Whall, D.R. Leadley, Ultra-high hole mobility exceeding one million in a strained germanium quantum well, Appl. Phys. Lett. 101 (2012) 172108.
[8] M. Myronov, C. Morrison, J. Halpin, S. Rhead, C. Casteleiro, J. Foronda, V.A. Shah, D. Leadley, An extremely high room temperature mobility of two-dimensional holes in a strained Ge quantum well heterostructure grown by reduced pressure chemical vapor deposition, Jpn. J. Appl. Phys. 53 (2014), 04EH02.
[9] M. Myronov, C. Morrison, J. Halpin, S. Rhead, J. Foronda, D. Leadley, Revealing high room and low temperatures mobilities of 2D holes in a strained Ge quantum well heterostructures grown on a standard Si(001) substrate, Solid State Electron. 110 (2015) 35–39.
[10] S. Datta, B. Das, Electronic analog of the electro-optic modulator, Appl. Phys. Lett. 56 (1990) 665.
[11] Y.A. Bychkov, E.I. Rashba, Oscillatory effects and the magnetic susceptibility of carriers in inversion layers, J. Phys. C Solid State Phys. 17 (1984) 6039–6045.
[12] C. Morrison, P. Wiśniewski, S.D. Rhead, J. Foronda, D.R. Leadley, M. Myronov, Observation of Rashba zero-field spin splitting in a strained germanium 2D hole gas, Appl. Phys. Lett. 105 (2014) 182401.
[13] J. Foronda, C. Morrison, J.E. Halpin, S.D. Rhead, M. Myronov, Weak antilocalization of high mobility holes in a strained germanium quantum well heterostructure, J. Phys. Condens. Matter 27 (2014) 022201.
[14] R. Moriya, K. Sawano, Y. Hoshi, S. Masubuchi, Y. Shiraki, A. Wild, C. Neumann, G. Abstreiter, D. Bougeard, T. Koga, T. Machida, Cubic Rashba spin–orbit interaction of a two-dimensional hole gas in a strained-Ge/SiGe quantum well, Phys. Rev. Lett. 113 (2014) 086601.
[15] G. Dresselhaus, Spin–orbit coupling effects in zinc blende structures, Phys. Rev. 100 (1955) 580–586.

[16] V.A. Shah, A. Dobbie, M. Myronov, D.J.F. Fulgoni, L.J. Nash, D.R. Leadley, Reverse graded relaxed buffers for high Ge content SiGe virtual substrates, Appl. Phys. Lett. 93 (2008) 192103.
[17] P.T. Coleridge, R. Stoner, R. Fletcher, Low-field transport coefficients in GaAs/$Ga_{1-x}Al_xAs$ heterostructures, Phys. Rev. B 39 (1989) 1120–1124.
[18] I.B.B. Yu, F. Komnik, V.V. Andrievskiĭ, O.A. Mironov, M. Myronov, D.R. Leadley, Quantum effects in hole-type Si/SiGe heterojunctions, Low Temp. Phys. 26 (2000) 609.
[19] R. Winkler, Spin–orbit Coupling Effects in Two-dimensional Electron and Hole Systems, Springer-Verlag, 2003.
[20] B. Grbić, R. Leturcq, T. Ihn, K. Ensslin, D. Reuter, A.D. Wieck, Strong spin–orbit interactions and weak antilocalization in carbon-doped p-type GaAs/$Al_xGa_{1-x}As$ heterostructures, Phys. Rev. B 77 (2008) 125312.
[21] M. Failla, M. Myronov, C. Morrison, D.R. Leadley, J. Lloyd-Hughes, Narrow heavy-hole cyclotron resonances split by the cubic Rashba spin–orbit interaction in strained germanium quantum wells, Phys. Rev. B 92 (2015) 045303.